

# Current induced torques and interfacial spin-orbit coupling: Semiclassical Modeling

Paul M. Haney,<sup>1</sup> Hyun-Woo Lee,<sup>2</sup> Kyung-Jin Lee,<sup>3,4,1,5</sup> Aurélien Manchon,<sup>6</sup> and M. D. Stiles<sup>1</sup>

<sup>1</sup>*Center for Nanoscale Science and Technology, National Institute of Standards and Technology, Gaithersburg, Maryland 20899-6202, USA*

<sup>2</sup>*PCTP and Department of Physics, Pohang University of Science and Technology, Kyungbuk 790-784, Korea*

<sup>3</sup>*Korea University, Department of Material Science & Engineerin, Seoul 136701, South Korea*

<sup>4</sup>*Korea Institute of Science and Technology, Seoul 136-791, Korea*

<sup>5</sup>*Univeristy of Maryland, Maryland Nanocenter, College Pk, MD 20742 USA*

<sup>6</sup>*Core Labs, King Abdullah University of Science and Technology (KAUST), Thuwal 23955-6900, Saudi Arabia*

In bilayer nanowires consisting of a ferromagnetic layer and a non-magnetic layer with strong spin-orbit coupling, currents create torques on the magnetization beyond those found in simple ferromagnetic nanowires. The resulting magnetic dynamics appear to require torques that can be separated into two terms, damping-like and field-like. The damping-like torque is typically derived from models describing the bulk spin Hall effect and the spin transfer torque, and the field-like torque is typically derived from a Rashba model describing interfacial spin-orbit coupling. We derive a model based on the Boltzmann equation that unifies these approaches. We also consider an approximation to the Boltzmann equation, the drift-diffusion model, that qualitatively reproduces the behavior, but quantitatively fails to reproduce the results. We show that the Boltzmann equation with physically reasonable parameters can match the torques for any particular sample, but in some cases, it fails to describe the experimentally observed thickness dependences.

## I. INTRODUCTION

Spintronic applications like spin-transfer-torque magnetic random access memory (STT-MRAM) or magnetic domain wall-based devices require advances in materials to reach their full potential. The goal of improving these materials has led to the study of bilayers consisting of ferromagnetic layers and non-magnetic layers with strong spin orbit coupling. Recent measurements on such systems have demonstrated efficient switching of magnetic tunnel junctions,<sup>1</sup> like those used in STT-MRAM, and efficient current-driven domain wall motion.<sup>2</sup>

There are a number of physical processes<sup>3</sup> in these systems that contribute to the magnetization dynamics as described by the Landau-Lifshitz-Gilbert equation. These include the typical micromagnetic contributions, like interatomic exchange, magnetostatic interactions, magnetocrystalline anisotropy, and damping, as well as the adiabatic and non-adiabatic spin transfer torques<sup>4–11</sup> that are typically added to account for the coupling between the magnetization and the electrical current flowing through it. In the bilayers of interest here, there are additional contributions that have received extensive attention. These arise from the spin-orbit coupling in the non-magnetic layer and from the enhanced spin-orbit coupling at the interfaces between layers.

These additional contributions have been modeled in terms of two different pictures. One picture<sup>12</sup> assumes that the layers are thick and the two layers have their bulk properties. A current flowing through the non-magnetic layer with strong spin-orbit coupling generates a spin current perpendicular to the interface (the spin Hall effect.<sup>13–16</sup>) When this spin current impinges on the interface, there is a spin transfer torque<sup>17–20</sup> on the magnetization of the magnetic layer. The details of the torque in this picture are determined by the bulk spin Hall angle

in the material with strong spin-orbit coupling and the mixing conductance. The other picture<sup>21–24</sup> assumes two dimensional transport that can be described by a Rashba model, similar to those used to describe spin-orbit coupling in two-dimensional electron gases.<sup>25</sup> The Rashba model gives direct coupling between the magnetization and the flowing current. Both models give qualitatively similar results, that is torques along the  $\mathbf{M} \times (\mathbf{j} \times \hat{\mathbf{z}})$  and  $\mathbf{M} \times [\mathbf{M} \times (\mathbf{j} \times \hat{\mathbf{z}})]$  directions, where  $\mathbf{M}$  is the magnetization,  $\mathbf{j}$  is the in-plane current density and the interface normal is in the  $\hat{\mathbf{z}}$  direction. We refer to the first torque as a field-like torque because it has the same form as precessional torque around an effective field in the  $-\mathbf{j} \times \hat{\mathbf{z}}$  direction. The second torque has the same form as a damping torque toward a field in that same direction and we refer to it as a damping-like torque.<sup>26</sup>

Both models have strengths and weaknesses. The Rashba model treats the strong spin-orbit coupling at the interfaces between the materials but treats the transport as two-dimensional. The layer thicknesses are usually comparable to mean free paths and spin diffusion lengths requiring a three dimensional description of the transport. On the other hand, the spin-Hall-effect spin-transfer-torque model treats the three dimensional aspect of the transport, but ignores any contributions from the modification of the spin-orbit coupling near the interface. The non-magnetic layer and the magnetic layer affect the electronic structure of each other close to the interface and the interaction can significantly change the spin-orbit coupling there. In particular, the proximity to the ferromagnet can induce a moment in the material with strong spin-orbit coupling giving a thin layer where the magnetism and the spin-orbit coupling coexist.<sup>27</sup>

Attempts to develop predictive models face the complication that the experimental structures deviate significantly from the ideal structures treated theoretically. Ex-

perimental indications<sup>28,29</sup> that interfaces of Co grown on Pt have different properties than interfaces of Pt grown on Co argue strongly that the details of the interface structure are both nontrivial and important. Unfortunately, the interfaces are not well enough characterized to know what types of disorder might be present. There may be significant interdiffusion at the interfaces because, for example, Pt alloys with Co in the bulk. There is also significant lattice mismatch between the materials. This mismatch could promote thickness fluctuations and dislocation formation. Without measurements of atomic scale structure of the experimental samples, it is impossible to know how important such defects are to the behavior of the system.

Motivated by the uncertainty in the details of the experimental structures and the goal of incorporating the strengths of existing models, we develop simple semiclassical models for these systems. One approach is based on the Boltzmann equation and the other on the drift-diffusion equation. Both capture the essential physics of the models that have been used so far and provide a test for whether a model based on bulk properties and enhanced spin-orbit coupling at the interface can account for the experimental behavior. We find that these models are general enough to reproduce the torques measured in any single sample for reasonable values of the parameters, but not all samples with a single parameterization. In Sec. II we summarize the experimental evidence for the different interpretations. We also summarize the micromagnetic simulations that provide the basis for these interpretations. We briefly present the semiclassical transport models in Sec. III and then apply them in Sec. IV to the model for a bulk spin Hall current in the non-magnetic layer leading to a spin transfer torque at the interface with the ferromagnet. In Sec. V we add in the interfacial spin orbit coupling and show that this captures the important physics that is included in the Rashba-model approaches.

## II. EXPERIMENTAL RESULTS AND THEORETICAL IMPLICATIONS

Recent experiments on multi-layer structures report evidence for current-induced torques due to spin-orbit coupling. These torques are reported to be large enough to modify the magnetization dynamics and may be utilized to facilitate spintronic applications. Various experiments report conflicting results for the size and direction of the torque. Many of these values are inferred from measurements of the resulting dynamics in conjunction with simulations. This section aims to summarize the evidence from experiments, in conjunction with simulations, for different forms of the torque.

The recent growth of interest in bilayer systems began with a series of experiments by Liu *et al.*<sup>1,30-32</sup> and Miron *et al.*<sup>2,33,34</sup> Both sets of experiments treat systems of a substrate, non-magnetic layer, ferromagnetic layer, and

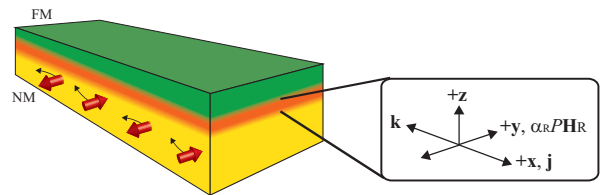


FIG. 1: (color online) Schematic of a bilayer structure that consists of a ferromagnetic layer and a non-magnetic metal layer with strong spin-orbit coupling. The spin Hall effect in the non-magnetic layer bends electron trajectories and injects electrons with proper spin direction into the adjacent magnetic layer, thereby generating the damping like torque. In this illustration, the spin Hall angle for the non-magnetic layer is assumed to be positive. The figure also highlights the interface region between the two layers, where the Rashba spin-orbit coupling may have sizable magnitude.

capping layer, see Fig. 1, although the details of each differ from experiment to experiment. The authors of the first set of experiments interpret their results in terms of a dominant damping like torque that they attribute to the spin Hall effect and as subsequent spin transfer torque. On the other hand, the authors of the second set of experiments interpret their results in terms of an important field like torque that they attribute to interfacial spin orbit coupling.

In the case of the spin Hall effect, electron trajectories are preferentially scattered in different directions depending on their spin directions. For instance, in a non-magnetic material with positive spin Hall angle, electrons are scattered more strongly into directions such that  $(\mathbf{v}_i \times \mathbf{v}_f) \cdot \mathbf{S}$  is positive, where  $\mathbf{v}_{i(f)}$  is the electron velocity before (after) the scattering and  $\mathbf{S}$  is the electron spin direction. Thus in the bilayer system in Fig. 1, the spin Hall effect in the non-magnetic layer injects electrons with spin along  $+\hat{\mathbf{y}}$  direction into a magnetic layer if  $\hat{\mathbf{j}}$  is along  $+\hat{\mathbf{x}}$  direction and the spin Hall angle is positive. As it does for perpendicular flow of electrons in multilayer systems, this spin current causes spin transfer torques,<sup>17-20</sup> the injected electrons giving rise to a spin torque along the direction  $-\mathbf{M} \times (\mathbf{M} \times \mathbf{m})$ , where  $\mathbf{m}$  is the direction of the magnetic moment carried by injected electrons and points along  $-\hat{\mathbf{y}}$  direction since  $\mathbf{m}$  and  $\mathbf{S}$  are anti-parallel. This torque amounts to the damping-like torque  $-\mathbf{M} \times [\mathbf{M} \times (\hat{\mathbf{j}} \times \hat{\mathbf{z}})]$  arising from the spin Hall effect.

Liu *et al.* examine various magnetization dynamics caused by the spin Hall effect. In Pt/Py bilayer,<sup>30</sup> they use the spin-torque ferromagnetic resonance technique to show that the spin Hall effect is strong enough to cause magnetic precession. Through the resonance line shape analysis, they quantify the magnitude of the spin-Hall-effect-induced damping like torque and the torque due to the Oersted field. They estimate the spin Hall angle of Pt to be about  $+0.076$ , which is about two orders of magnitude larger than the correspond-

ing value in  $n$ -doped GaAs.<sup>35,36</sup> This demonstrates that the spin Hall effect can be a realistic tool to enhance spin torque efficiency. In their subsequent work<sup>1</sup> for the Ta/Co<sub>40</sub>Fe<sub>40</sub>B<sub>20</sub> bilayer, they demonstrate that the spin-Hall-induced damping-like torque can switch the magnetization in a reliable and efficient way, facilitating the development of magnetic memory and nonvolatile spin logic technologies. From three different measurements (spin-torque ferromagnetic resonance, current-dependent anomalous Hall effect, threshold current density for magnetization switching), they estimate the spin Hall angle of Ta to be  $-0.12$  to  $-0.15$ . This angle is of opposite sign compared to Pt but most notably, larger by about a factor of two. In their still later work,<sup>31</sup> they demonstrate that the magnetization switching can be achieved by the spin Hall effect in Pt(2 nm)/Co(0.6 nm)/AlO<sub>x</sub> systems as well, although the spin Hall angle in Pt is smaller. Most recently, they have determined an even larger spin Hall angle in W.<sup>37</sup>

On the other hand, Miron *et al.*<sup>2,33,34</sup> explore effects of the Rashba spin-orbit coupling with focus on the system Pt(3 nm)/Co(0.6 nm)/AlO<sub>x</sub>(2 nm). The layer structure of the film breaks inversion symmetry and gives rise to perpendicular magnetic anisotropy strong enough that the ground state for the magnetization is out of plane. In these experiments, the nominally symmetric control system Pt(3 nm)/Co(0.6 nm)/Pt(3 nm), shows much weaker effects, leading to the inference that the broken inversion symmetry for the layer plays a crucial role.

Miron *et al* interpret their results in terms of a large field-like torque as expected from the Rashba model<sup>25</sup> for interfacial spin-orbit coupling. Calculations<sup>21–24</sup> predict an effective field<sup>38</sup>

$$\mu_0 \mathbf{H}_R \approx \frac{\alpha_R}{2\mu_B M_s} P(\hat{\mathbf{z}} \times \mathbf{j}), \quad (1)$$

when a system is subject to the Rashba spin-orbit coupling of the form  $\alpha_R(\mathbf{k} \times \hat{\mathbf{z}}) \cdot \boldsymbol{\sigma}$ . Here  $M_s$  is the saturation magnetization,  $P$  is the spin polarization, and  $\mu_B$  is the Bohr magneton. The effective field  $\mathbf{H}_R$  generates the field-like torque  $-\gamma \mathbf{M} \times \mathbf{H}_R \propto -\mathbf{M} \times (\hat{\mathbf{z}} \times \mathbf{j})$ , where  $\gamma$  is the gyromagnetic ratio.

In Ref. 33, the authors measure the reversal of the perpendicular magnetization. They find that transverse in-plane magnetic fields enhance the nucleation and that this enhancement is modified by currents flowing through the film. In-plane currents  $\mathbf{j}$  flowing through the system enhance (suppress) the nucleation of reversed magnetic domains when the direction  $\hat{\mathbf{z}} \times \mathbf{j}$  is parallel (anti-parallel) to externally applied in-plane magnetic fields. In the nominally symmetric control sample, the effect of in-plane current is much weaker. The authors interpret the effect of in-plane currents as evidence for the current-induced effective field along  $\hat{\mathbf{z}} \times \mathbf{j}$ , as predicted theoretically for systems with Rashba-like spin orbit coupling. Experimentally,<sup>33</sup> the magnitude of the effective field is proportional to  $\mathbf{j}$  with a proportionality constant  $(1.0 \pm 0.1) \times 10^{-12} \text{ T}/(\text{A} \cdot \text{m}^{-2})$ . This value implies  $\alpha_R \approx$

$0.2 \text{ eVnm}$ ,<sup>39</sup> which is comparable to  $\alpha_R = 0.3 \text{ eVnm}$  reported for Bi/Ag(111) surface<sup>40</sup> and comparable to a recent first principles calculation result for a Pt/Co bilayer.<sup>41</sup>

Further evidence for a field-like torque is found in measurements<sup>2</sup> of current-driven domain wall (DW) motion in the same system. As the driving current density goes up, the domain wall velocity  $v_{\text{DW}}$  increases to speeds up to  $\approx 400 \text{ m/s}$ , more than three times faster than previously measured current-driven domain wall velocities.<sup>42</sup> The authors claim that this velocity is twice as large as the rate  $v_s = |\mathbf{j}|(Pg\mu_B)/(2eM_s)$  of the spin angular momentum transfer, where  $g(\approx 2)$  is the gyromagnetic ratio. Even up to such high domain wall speeds, the domain walls apparently did not undergo structural instability (Walker breakdown.<sup>43,44</sup>) According to conventional theories<sup>6,8</sup> of current-driven domain wall motion, domain wall velocities above  $v_s$  are possible below the breakdown current density  $j_W$ . However, as the ratio  $v_{\text{DW}}/v_s$  increases, the breakdown current density decreases such that conventional theories cannot explain the velocities measured in this experiment.<sup>2</sup>

As a possible explanation, the authors suggest<sup>2</sup> that the current-induced effective field  $\mathbf{H}_R$  could increase the breakdown current density. Consider the two low energy structures [Figs. 2(a) and (b)] of the Bloch domain wall. These walls differ from each other because they have opposite magnetization directions at the domain wall center. Since the two directions are parallel and anti-parallel to  $\mathbf{H}_R$ , the effective field either stabilizes or destabilizes the corresponding Bloch domain wall structures [Fig. 2(d)]. Recalling that the conventional spin torques produced by the current tend to shift<sup>8</sup>  $\phi$  away from the low energy values ( $\phi = 0$  and  $\pi$ ), the deeper energy valley implies an enhanced threshold current density to escape the valley. Since the Walker breakdown occurs when  $\phi$  cannot remain stationary, the Walker breakdown threshold current density becomes the larger of the two, which is larger than the Walker breakdown threshold value without  $\mathbf{H}_R$ .

Another interesting feature of the experiment<sup>2</sup> is that contrary to previous experiments,<sup>42,45,46</sup> which report domain wall motion along the electron flow direction, Ref. 2 reports domain wall motion *against* the electron flow. Within the scope of the conventional theories,<sup>6,8</sup> the reversed domain wall motion implies negative  $P\beta$ , where  $P$  is the polarization of the current and  $\beta$  is the dimensionless coefficient of the non-adiabatic spin transfer torque. All of the qualitative feature of the experiment<sup>2</sup> would be explained if there were an  $\mathbf{H}_R$  that gives Walker breakdown threshold enhancement, negative  $P\beta$  for reversed motion, and  $|\beta/\alpha| > 1$  for velocity enhancement ( $\alpha$  is the Gilbert damping constant).

Further measurements<sup>34</sup> on the same Pt(3 nm)/Co(0.6 nm)/AlO<sub>x</sub>(1.6 nm) system reveal a problem in this simple theoretical picture. Based on measurements of bipolar switching in a tilted field, the authors conclude that the switching is due the

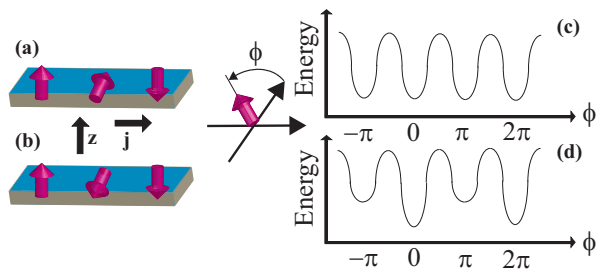


FIG. 2: (color online) Two possible structures of the Bloch domain wall. In (a), the magnetization at the center of the domain wall points along  $\hat{z} \times \mathbf{j}$  and in (b), it points along  $-\hat{z} \times \mathbf{j}$ . Panel (c) shows the domain wall energy as a function of the domain wall tilting angle  $\phi$  without the effective field  $\mathbf{H}_R$ . Panel (d) shows the energy with the effective field assuming that  $\alpha_R P$  is positive and  $\mathbf{H}_R$  prefers  $\phi = 0$ .

additional presence of a damping-like torque along  $\mathbf{M} \times [\mathbf{M} \times (\hat{z} \times \mathbf{j})]$ . The damping-like torque is either parallel or anti-parallel to the nonadiabatic STT at the domain wall center and thus modifies the domain wall velocity.<sup>47,48</sup> A recent theoretical study<sup>47</sup> demonstrates that high  $v_{DW}$  *against* electron flow direction is possible (Fig. 3) even when both  $P$  and  $\beta$  are positive and  $\beta/\alpha$  is smaller than 1, if both the field-like torque  $-\mathbf{M} \times (\hat{z} \times \mathbf{j})$  and the damping-like torque  $\mathbf{M} \times [\mathbf{M} \times (\hat{z} \times \mathbf{j})]$  are sufficiently large.

Miron *et al.*<sup>34</sup> estimate that the spin Hall contribution<sup>31</sup> to the damping-like torque is not strong enough to explain the bipolar switching and conclude that the damping-like torque arises mainly from the Rashba spin-orbit coupling, based on the observation that the efficiency of the bi-polar switching increases with the magnetic anisotropy of the cobalt layer and the oxidation of the aluminum layer. Calculations<sup>3,47,49,50</sup> confirm that the Rashba spin-orbit coupling can give rise to the damping-like torque. Note however that the spin Hall contribution and the Rashba spin-orbit coupling contribution to the damping-like torque have exactly the same structure, making the distinction difficult. In this regard, recent micromagnetic calculations<sup>47</sup> show that the spin Hall effect and the Rashba spin-orbit coupling contributions give qualitatively different domain wall motion if there is no field-like torque as might be expected if the spin Hall effect is the dominant source of the effect. Without the field-like torque, the domain wall motion at high current densities is along the electron flow direction (if  $\beta P > 0$ ) whereas with the strong field-like torque, the domain wall motion against the electron flow is possible even for  $\beta P > 0$  (solid line in Fig. 3).

In contrast to Miron *et al.*'s interpretation,<sup>34</sup> Liu *et al.*<sup>31</sup> conclude that the damping-like torque in Pt(2.0 nm)/Co(0.6 nm)/Al(1.6 nm) arises mainly from the spin Hall effect in Pt and the Rashba spin-orbit coupling contribution is negligible. As evidence for the lat-

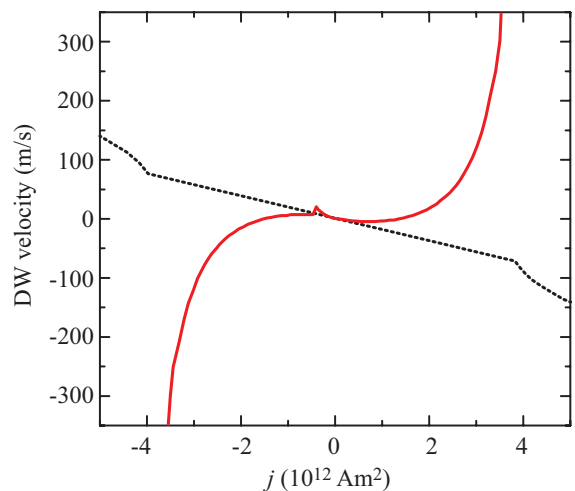


FIG. 3: (color online) Terminal domain wall velocity  $v_{DW}$  as a function of the current density  $\mathbf{j} = j\hat{x}$ . The dotted line gives the prediction of the Landau-Lifshitz-Gilbert equation when the current generates only the conventional (adiabatic and nonadiabatic) spin transfer torques and the solid line the prediction when the current also generates field-like and damping-like torques. For this calculation, we consider a nanostrip of length  $\times$  width  $\times$  thickness = 2000 nm  $\times$  200 nm  $\times$  5 nm, with perpendicular magnetic anisotropy and the materials parameters as follows:  $\gamma/(2\pi) = 28$  GHz/T,  $M_s = 1 \times 10^6$  A/m,  $A_{ex} = 1.3 \times 10^{-11}$  J/m,  $P = 0.7$ ,  $K_u = 1.5 \times 10^6$  J/m<sup>3</sup>,  $\alpha = 0.5$ ,  $\beta = 0.25$ , and  $\alpha_R = 0.7 \times 10^{-10}$  eV.m. For the conventional calculation (dotted curve), the non-linearities are due to Walker breakdown. In the solid curve, the small blip at a small negative current is caused by the chirality switching of domain wall due to the spin-orbit-related field-like torque.

ter conclusion, they report that the ratio between the current-induced effective field along  $\hat{z} \times \mathbf{j}$  and the in-plane current density is more than 75 times smaller than the corresponding ratio in Ref. 33. A third experiment<sup>51</sup> on a similar system Pt(3.0 nm)/Co(0.6 nm)/AlO<sub>x</sub>(1.8 nm) found that this ratio is about 3.4 times smaller than the ratio reported in Ref. 33.

Experiments<sup>52</sup> that measure the field-like torque on Ta(1.0 nm)/Co<sub>40</sub>Fe<sub>40</sub>B<sub>20</sub>(1.0 nm)/MgO(2.0 nm) find that the ratio of the effective field to the current is about 23 % of the corresponding ratio in Pt/Co/AlO<sub>x</sub> as reported in Ref. 33. Interestingly, the current-induced effective field in the Ta/CoFeB/MgO system is along  $-\hat{z} \times \mathbf{j}$  and thus opposite to the corresponding direction in the Pt/Co/AlO<sub>x</sub> system if the Ta and MgO layers in the Ta/CoFeB/MgO system are matched with Pt and AlO<sub>x</sub> layers in the Pt/Co/AlO<sub>x</sub> system, respectively. It was also reported that the torque to current ratio decreases by more than an order of magnitude when the thickness of the Co<sub>40</sub>Fe<sub>40</sub>B<sub>20</sub> layer in the Ta/CoFeB/MgO system increases slightly from 1.0 nm to 1.2 nm.

The thickness dependence was investigated systematically<sup>53</sup> for the two wedge systems,

Ta( $d_{\text{Ta}}$ )/Co<sub>20</sub>Fe<sub>60</sub>B<sub>20</sub>(1 nm)/MgO(2 nm) and Ta(1 nm)/Co<sub>20</sub>Fe<sub>60</sub>B<sub>20</sub>( $t_{\text{CoFeB}}$ )/MgO(2 nm). When the Ta layer thickness  $d_{\text{Ta}}$  changes by 1 nm, the effective field along the  $\hat{\mathbf{z}} \times \mathbf{j}$  direction changes its magnitude by nearly two orders of magnitude. For small  $d_{\text{Ta}} \lesssim 0.6$  nm, the sign of the effective field is opposite to that in the larger  $d_{\text{Ta}}$  regime and agrees with the sign of the Pt/Co/AlO<sub>x</sub> system.<sup>33</sup> The damping-like effective field along the  $(\hat{\mathbf{z}} \times \mathbf{j}) \times \mathbf{M}$  direction is also sensitive to  $d_{\text{Ta}}$  with the sign change at  $d_{\text{Ta}} \approx 0.5$  nm. The sign change of the damping-like effective fields is interpreted as an evidence of competition between Rashba spin-orbit coupling and spin Hall effect.<sup>1</sup>

Measurements of current-driven domain wall motion in multi-layer structures containing non-magnetic heavy metal layers and ferromagnetic layers but without oxide layers<sup>29,54</sup> are reported. The motion is also very sensitive to layer thicknesses.<sup>29</sup> The domain wall velocity can be up to almost 1 km/s in certain multi-layer structures with the Pt layer thickness of about 1 nm but changes very quickly as the Pt thickness varies. Interestingly, very high domain wall speed ( $\approx 1$  km/s) are observed only when the domain wall moves against the electron flow, implying that the origin of the reversed domain wall motion is probably correlated with the mechanism behind very high domain wall speed. Several other experiments<sup>28,55-57</sup> also report reversed domain wall motion in ultrathin multi-layer systems containing Pt layers.

The analysis of domain wall motion described above considers four current induced torques, the the adiabatic and non-adiabatic spin-transfer torques and two torques, damping-like and field-like, that depend on the layer structure of the device. The first two torques depend on the gradient of the magnetization but are determined by bulk properties. The last two are independent of the gradient of the magnetization. Other possibilities that depend on the gradient of the magnetization and the layer structure are allowed by symmetry<sup>3</sup> and may be important for the dynamics. In addition, recent calculations<sup>58</sup> suggest that a current-independent torque due to the Dzyaloshinskii-Moriya interaction<sup>59</sup> might provide an alternate mechanism for stabilizing a moving domain wall above the nominal Walker-breakdown field. In this paper we only consider the current-induced torques that are independent of the gradient of the magnetization.

### III. SEMICLASSICAL MODELS

To explore possible mechanisms for the torques operative in these systems, we develop semiclassical models that allow for easy exploration of parameter space. We use a Boltzmann equation approach and the simpler drift-diffusion approach. The Boltzmann equation is better suited to describe in-plane transport but the drift-diffusion approach is simpler and provides a useful language to describe the physics.

The Boltzmann equation approach developed by Cam-

ley and Barnas<sup>60</sup> is the simplest model that describes current-in-the-plane (CIP) giant-magnetoresistance (GMR). In the Boltzmann equation, the variables are the distribution functions. The distribution function accounts for electrons moving in all directions even though the total current only points in a single direction. This generality allows the approach to describe the flow of spins between the layers even though the current flows in the plane of the interfaces.

The drift-diffusion approach of Valet and Fert<sup>61</sup> is based on integrating the distribution function in the Boltzmann equation to derive transport equations that depend on the densities and currents. It has had wide success describing current-perpendicular-to-the-plane (CPP) GMR, but does not describe CIP GMR. It fails because it does not describe the flow of spin currents between the layers when the current flows in the plane of the layers. However, this limitation may be less important in the bilayer systems of interest here. In materials with strong spin-orbit coupling, like Pt, spin currents do flow perpendicular to the charge current because of the spin Hall effect<sup>62</sup> so that the drift-diffusion approach does qualitatively describe the physics. However, we compare the two approaches below, and show that the drift-diffusion approach differs quantitatively from the Boltzmann equation for similar reasons to its qualitative failure for CIP GMR.

Reference 63 describes the matrix Boltzmann equation we use in this paper. It is a generalization of the model used to describe CIP GMR,<sup>60</sup> and is based on a very simplified model for the electronic structure. We treat all Fermi surfaces as spherical and as having the same Fermi wavevector. This approach ignores the details of the Fermi surfaces, which are undoubtedly important for specific systems, particularly when including spin-orbit coupling. However, the scattering mechanisms are both unknown and uncharacterized, so we feel that it is appropriate to consider models in which scattering rates and other physical processes are parameterized and the details of the electronic structure are neglected for simplicity. By performing appropriate integrals over the distribution function, the Boltzmann equation can be transformed into a drift-diffusion equation like that given in Ref. 64. The parameterized processes in the Boltzmann equation then have a simple connection to those in the drift-diffusion equation.

One such process that we include through parameterization is the spin-dependent conductivity in the ferromagnetic layer. We model the spin dependence by using spin-dependent scattering rates. Such spin-dependent scattering is physically sensible as it is believed to play a bigger role in the polarization of the current in these materials than the electronic structure itself. For example, in Co and Ni, the current is expected to be dominated by majority carriers, even though there are more minority carriers at the Fermi surface. In the drift diffusion model, the spin-dependent scattering leads to a different conductivity for the majority electrons  $\sigma^\uparrow$  than the

minority electrons  $\sigma^\downarrow$ . This difference is parameterized in terms of the spin polarization of the current, defined through  $P = (\sigma^\uparrow - \sigma^\downarrow)/(\sigma^\uparrow + \sigma^\downarrow)$ . The drift-diffusion transport equations in the ferromagnet are

$$\mathbf{j} = \sigma \nabla \mu - P \sigma \nabla (\hat{\mathbf{M}} \cdot \boldsymbol{\mu}^s), \quad (2)$$

$$Q_{ij} = \frac{\hbar}{2e} \hat{M}_j P \sigma \nabla_i \mu - \frac{\hbar}{2e} \sigma \nabla_i \mu_j^s, \quad (3)$$

where  $\mathbf{j}$  is the charge current density, and  $\mathbf{Q}$  is the tensor spin current density where the first index is the spatial component and the second index the spin component.  $\mu$  is the electrochemical potential, such that negatively charged electrons diffuse against the gradient giving an overall positive sign for the first term in Eq. (2). Similarly  $\boldsymbol{\mu}^s$  is the spin chemical potential, which is a vector along the direction of the spin accumulation, and the unit vector  $\hat{\mathbf{M}}$  is the direction of the magnetization. The minus sign in the second term of Eq. (2) arises because majority electron spins are aligned opposite to the magnetization. These two signs are typical of possible sources of confusion in this subject matter. They arise because with the charge on the electron is negative and angular momenta and moments are in opposite directions.

The equality of the Fermi surfaces would also allow for perfect transmission of electrons across the interface between the materials. In the Boltzmann equation, we include spin-dependent reflection by the addition of a spin-dependent sheet potential (delta function) at the interface. Choosing the strength of this delta function allows us to tune the spin-dependent interface resistance to any arbitrary value.<sup>66</sup> In the drift-diffusion approach, the spin-dependent reflection becomes a spin-dependent interface resistance or conductance as used in the closely related circuit theory.<sup>67</sup>

While the overall structure of the Boltzmann equation approach is the same as that published earlier, there are some modifications. One difference is the treatment of dephasing. In a ferromagnet, spins on different parts of the Fermi surface precess at different rates and travel with different velocities. These differences, combined with scattering between different parts of the Fermi surface, cause the precessing spins to rapidly become out of phase with each other.<sup>68</sup> In Ref. 63, the transverse spin accumulation and current are forced to zero in the ferromagnet to account for this dephasing of the transverse spin population. Here, we allow for transverse spin accumulation in the ferromagnet but build in rapid spin precession and explicitly account for the processes that cause dephasing. The simplified model of the Fermi surfaces that we use can lead to underestimation of dephasing processes. We have tested this approximation by adding an explicit dephasing term. While such a term quantitatively changes the spin accumulation in the ferromagnet, we find that it does not change the calculated torques.

The same dephasing process is absent in a drift-diffusion model but can be included by adding an explicit dephasing term. In this approximation, the steady-state

continuity equations in the ferromagnet are

$$\nabla \cdot \mathbf{j} = 0 \quad (4)$$

$$\begin{aligned} \nabla_i Q_{ij} = & -\frac{1}{\tau_{\text{ex}}} (\mathbf{s} \times \hat{\mathbf{M}})_j - \frac{1}{\tau_{\text{sf}}} s_j \\ & - \frac{1}{\tau_{\text{dp}}} \left[ \hat{\mathbf{M}} \times (\mathbf{s} \times \hat{\mathbf{M}}) \right]_j \end{aligned} \quad (5)$$

where the spin accumulation  $\mathbf{s}$  is proportional to the spin chemical potential  $\mathbf{s} = \mathcal{N}_s \boldsymbol{\mu}^s$  and the precession time  $\tau_{\text{ex}} = \hbar/\Delta$  is related to the exchange splitting between the magnetization and the spin accumulation. Repeated indices are summed over. The first term on the right hand side of Eq. (5) is the precession in the exchange field, the second term is the spin flip scattering that reduces all components of the spin accumulation, and the last term is the dephasing that reduces only the parts of the spin accumulation transverse to the magnetization. Setting the transverse spin accumulation to zero, as done in earlier Boltzmann equation calculations<sup>63</sup> and in magnetoelectronic circuit theory,<sup>67</sup> is equivalent to taking the limit that the dephasing time goes to zero.

Both the size of the spin Hall effect and its underlying mechanism are controversial. The theory for the spin Hall effect is related to that for the anomalous Hall effect, a subject that has been controversial for decades.<sup>69</sup> Measurements of the spin Hall angle (the ratio of spin Hall and charge conductivities) for various materials span a range of values. Part of the variation may result from the sensitivity of the extraction of the spin Hall angle from experimental data to other material parameters needed to model the experiments.<sup>32</sup> Measurements<sup>1</sup> show that the spin Hall effect in Ta is bigger and of the opposite sign of that in Pt, in agreement with previous calculations.<sup>70</sup> The agreement between these trends in theory and experiment argues for an intrinsic origin of the effect. However, the calculated spin Hall conductivity for Pt appears to be approximately an order of magnitude too small in comparison to the measured value. Spin Hall angles of approximately the right order of magnitude have been computed<sup>71</sup> for the extrinsic contributions of various impurities in Cu and Au.

With this uncertainty in the mechanism for the spin Hall effect, we use the form of scattering appropriate for the extrinsic skew scattering contribution for computational simplicity. In the Boltzmann equation, we include skew scattering as described by Engel et al.<sup>36</sup> but generalize their results to include scattering that leads to the inverse spin Hall effect in addition to the scattering that gives rise to the spin Hall effect. These scattering terms connect the current with a perpendicular spin current and vice versa. Both our approach and the earlier work<sup>36</sup> neglect the scattering processes that couple spin currents to spin currents moving in other directions. Such process contribute to spin relaxation, which we include as a phenomenological spin flip scattering process. Details of the scattering and the default parameters we use are given in Appendix A.

In the non-magnetic material, the explicit forms of the charge and spin currents in the drift-diffusion approximation we use are<sup>64</sup>

$$\mathbf{j} = \sigma \nabla \mu - \sigma_{\text{SH}} (\nabla \times \boldsymbol{\mu}^{\text{s}}), \quad (6)$$

$$Q_{ij} = -\frac{\hbar}{2e} \sigma \nabla_i \mu_j^{\text{s}} - \frac{\hbar}{2e} \sigma_{\text{SH}} \epsilon_{ijk} \nabla_k \mu. \quad (7)$$

where  $\sigma$  is the conductivity,  $\sigma_{\text{SH}}$  is the spin Hall conductivity coupling the spin and charge currents to the charge and spin potentials, and  $\epsilon_{ijk}$  is the Levi-Civita symbol. As with the Boltzmann equation, we neglect a term corresponding to the spin Hall effect coupling the spin current to the spin potential, assuming that it is small.

In both models, the torque on the magnetization is given by the torque between the magnetization and the spin accumulation

$$\mathbf{T} = \frac{\gamma}{\tau_{\text{ex}} M_{\text{s}}} \mathbf{M} \times \mathbf{s} + \frac{\gamma}{\tau_{\text{dp}} M_{\text{s}}} \mathbf{M} \times (\mathbf{M} \times \mathbf{s}), \quad (8)$$

where the gyromagnetic ratio  $\gamma = g\mu_{\text{B}}/\hbar$  converts from angular momentum (spin density) to magnetization (so  $\mathbf{T}$  is a term in the Landau-Lifshitz-Gilbert equation<sup>26</sup>). The second term, which is not present in the Boltzmann equation calculations, captures the torque due to the dephasing of the electron spins as they precess in the exchange field.

If there is no coupling of angular momentum into the lattice (spin-orbit coupling or spin-flip scattering) it is straightforward to relate this torque, Eq. (8), to the divergence of the spin current. In the ferromagnet, where there is spin-flip scattering but no other spin-orbit coupling, the corrections to torque being simply the divergence of the spin current can be found from Eq. (5). For the components perpendicular ( $\perp$ ) to the magnetization, the torque is

$$\begin{aligned} \mathbf{T} &= -\gamma(1-\beta)(\nabla \cdot \mathbf{Q})_{\perp} + \gamma\beta \hat{\mathbf{M}} \times (\nabla \cdot \mathbf{Q}), \\ \beta &= \frac{\tau_{\text{ex}}}{\tau_{\text{sf}}} \frac{1}{1+\xi^2}, \quad \xi = \frac{\tau_{\text{ex}}}{\tau_{\text{dp}}} + \frac{\tau_{\text{ex}}}{\tau_{\text{sf}}}, \end{aligned} \quad (9)$$

where  $(\nabla \cdot \mathbf{Q})_{\perp} = -\hat{\mathbf{M}} \times [\hat{\mathbf{M}} \times (\nabla \cdot \mathbf{Q})]$  is the component of the divergence of the spin current that is perpendicular to the magnetization. Equation (9) indicates that the spin torque is in general not simply given by the divergence of the spin current but possesses an additional component  $\hat{\mathbf{M}} \times \nabla \cdot \mathbf{Q}$  arising from the presence of spin relaxation. For the parameter set used here,  $\beta$  is negligible.

An important difference with the previously published<sup>63</sup> formalism for the Boltzmann equation is the inclusion of spin-orbit coupling at the interface. This is done by including an additional term in the interface potential

$$V(\mathbf{r}) = \frac{\hbar^2 k_{\text{F}}}{m} \delta(z) \left[ u_0 + u_{\text{ex}} \boldsymbol{\sigma} \cdot \hat{\mathbf{m}} + u_{\text{R}} \boldsymbol{\sigma} \cdot (\hat{\mathbf{k}} \times \hat{\mathbf{z}}) \right], \quad (10)$$

where the interface is in the  $\hat{\mathbf{z}}$  direction at  $z = 0$ ,  $u_0$  is the spin-independent part of the potential,  $u_{\text{ex}}$  is the spin-dependent part of the potential that gives rise to spin-dependent reflection,  $u_{\text{R}}$  is the Rashba contribution, with  $\mathbf{k}$  being the wave vector of an electron scattering from the interface,  $k_{\text{F}}$  is the Fermi wave vector, and  $m$  is the electron mass. This additional term captures the form of spin-orbit coupling that is allowed for the simple electronic structure assumed here. For more realistic band structures, the form would be much more complicated. Unfortunately, it is difficult to compare  $u_{\text{R}}$  with the  $\alpha_{\text{R}}$  used in previous publications. Doing so requires a procedure for reducing the Hamiltonian for a three dimensional system to one for a two-dimensional system.

In Eq. (10), the last two terms can be combined to give a wave vector dependent field direction  $\hat{\mathbf{u}}(\mathbf{k})$  and strength  $u_{\text{eff}}(\mathbf{k})$  such that  $u_{\text{eff}}(\mathbf{k}) \hat{\mathbf{u}}(\mathbf{k}) = u_{\text{ex}} \hat{\mathbf{m}} + u_{\text{R}} \hat{\mathbf{k}} \times \hat{\mathbf{z}}$ . With respect to this direction, the majority and minority transmission and reflection amplitudes are

$$T = \frac{ik_z/k_{\text{F}}}{ik_z/k_{\text{F}} - (u_0 \pm u_{\text{eff}})} \quad (11)$$

$$R = \frac{u_0 \pm u_{\text{eff}}}{ik_z/k_{\text{F}} - (u_0 \pm u_{\text{eff}})} \quad (12)$$

Since both the magnitude and phase of the transmission and reflection amplitudes are different for the majority and minority spin components, an electron spin oriented along some arbitrary direction undergoes a finite rotation when transmitted or reflected. A part of the torque on the electron spin is due to the coupling to the exchange field and a part due to the spin-orbit coupling (Rashba contribution). The reaction torque on the magnetization can be computed from the exchange coupling between the spin density at the interface and the exchange field

$$\mathbf{T} = \delta(z) \frac{\gamma}{M_{\text{s}}} \left( \frac{\hbar k_{\text{F}} u_{\text{ex}}}{m} \right) \mathbf{s} \times \mathbf{M} \quad (13)$$

where the spin density  $\mathbf{s}$  is calculated from the incoming wave function and the transmission amplitudes. Since the potential is proportional to a delta function, the torque density diverges but is finite when integrated over a finite thickness.

The treatment we use for the interfacial spin-orbit coupling in the Boltzmann equation does not generalize easily to the drift-diffusion equation because there are not any wave vector dependent quantities in that model. It may be possible to define a generalization of the conductance matrix used in the magnetoelectronic circuit theory. In typical usage, the longitudinal spin components couple to each other and the transverse spin components couple to each other, but the longitudinal and transverse spin components do not couple. With the Rashba interaction included, all spin components would couple.

The Boltzmann equation based approach differs quite significantly from the approach used in which the system is modeled with a two dimensional Rashba model. In our

Boltzmann equation approach, electron spins get kicked when they pass through the interface, but they spend no time “in” the interface. In the Rashba model, the entire system is the interface so the electrons (and spins) are “in” the interface at all times. In this case, there is a spin accumulation that builds up in the interface. This spin accumulation gives rise to the strong field-like torque found in these models. In spite of this difference, we find that the both approaches give qualitatively similar torques.

The remaining difference with the previously published formalism for the Boltzmann equation is that the boundary conditions are different. The previous version treated perpendicular transport and here we treat in-plane transport. Here, the outer boundaries are perfectly reflecting, either diffusely, specularly, or somewhere in between.

#### IV. SPIN HALL EFFECT PLUS SPIN TRANSFER TORQUE

In this Section, we describe the behavior of the model in the absence of spin-orbit coupling at the interface. In this limit, the spin Hall effect in the non-magnetic layer generates a spin Hall current that propagates perpendicular to the interface with spins pointed perpendicular to both the interface normal and the direction of the current. When this spin current hits the interface with the ferromagnet, angular momentum is transferred from the flowing spins to the magnetization as is typical for spin transfer torques in magnetic multilayers.<sup>17,18,20</sup>

This process is shown in Fig. 4 based on calculations done with the Boltzmann equation described in Sec III. Parameter choices are given in Table I in Appendix A. Fig. 4 shows the currents, spin currents, and spin densities for a 4 nm ferromagnetic layer coupled to a 6 nm non-magnetic layer with the interface at  $z = 0$ . Panel (a) shows the distribution through the thickness of the films of the current flowing in the plane of the film (in the  $x$ -direction). The current is greater in the ferromagnetic layer because it has a higher conductivity than the non-magnetic layer for this choice of parameters. The current is suppressed close to the outer boundaries because we assume that the scattering from those interfaces is completely diffuse. In fact, the ferromagnetic layer is not thick compared to the mean free paths, so the current is suppressed through the thickness of the film. The spin current with spins aligned with the magnetization ( $z$ -direction) and moving in the plane also reduced from the bulk value, in fact more so than the current, so the polarization of the current is reduced from the bulk value. At the interface between the two materials, the current is enhanced in the lower conductivity layer due to electrons entering from the higher conductivity layer, and the current is reduced in the higher conductivity layer.

This modification of the current near the interface is not captured by a drift-diffusion model. It is one source of the quantitative disagreement between the models as

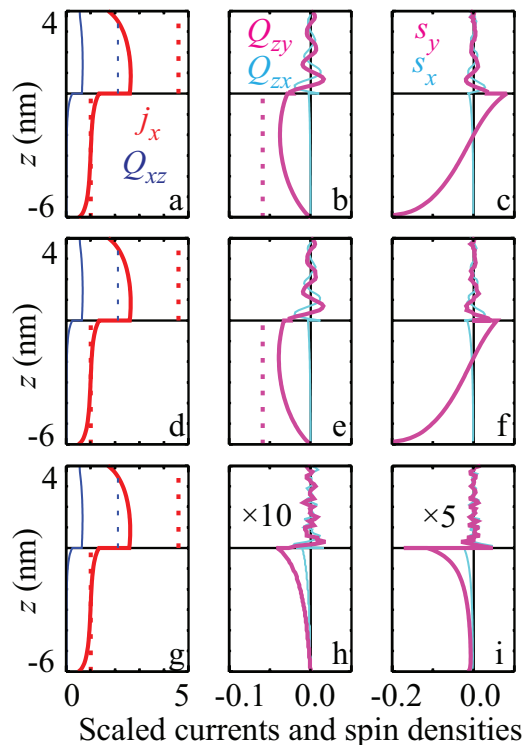


FIG. 4: (color online) Currents, spin currents, and spin accumulations. The left panels (a, d, and g) show the current density (heavy lines)  $j_x$ , which is flowing in the plane of the sample and the spin current  $Q_{xz}$  (lighter lines), flowing in the  $x$ -direction with spins aligned with the magnetization in the  $z$ -direction. The dotted lines indicate the bulk values. All currents and spin currents are dimensionless; currents are scaled by the bulk current in the non-magnet and spin currents are scaled by the bulk current in the non-magnet and an additional factor of  $\hbar/2e$ . The spin densities are scaled by the same factor two factors and  $v_F$ . The middle panels (b, e, and h) show the spin currents,  $Q_{zy}$  (heavy lines) and  $Q_{zx}$  (lighter lines), flowing perpendicular to the layers ( $z$ -direction) with spins pointing perpendicular to the magnetization, i.e. the  $x$ - and  $y$ -directions. The right panels (c, f, and i) show the accumulation of spin perpendicular to the magnetization,  $s_y$  (heavy lines) and  $s_x$  (lighter lines). The top panels (a, b, c) are for the case in which there is no interfacial spin orbit coupling, the bottom panels (g, h, i) for the case with interfacial spin-orbit coupling  $u_R = 0.04$  and no spin Hall effect in the non-magnet, and the middle panels (d, e, f) for the case when both are present. In panels (h) and (i), the spin accumulations have been scaled by the indicated factors.

discussed below.

Panel (b) of Fig. 4 shows the two components of the spin current with spins aligned perpendicular to the magnetization and moving perpendicular to the plane of the film. In the non-magnetic layer, this is due to the spin Hall effect. The spin current is zero at the lower boundary, which is both impenetrable and has no spin-flip scattering. It increases to close to its bulk value at the interface between the non-magnet and the ferromagnet. Inside the non-magnetic layer, the spin current is a compe-

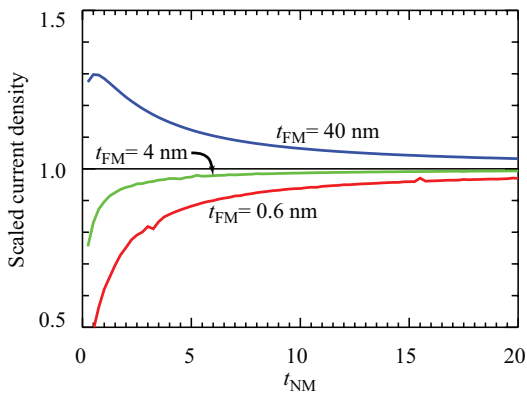


FIG. 5: (color online) Average current density in the non-magnetic layer. For three thicknesses of the ferromagnetic layer, the average current density in the non-magnetic layer is shown scaled by the bulk value as a function of the thickness of the non-magnetic layer.

tition between the spin Hall current and a diffusive spin current from the spin accumulation, seen in Panel (c), that builds up due to the impenetrability of the outer interface. Panels (d-i) show calculations with interfacial spin-orbit coupling included and are discussed in Sec. V.

At and near the interface, this spin current is converted into a spin transfer torque on the ferromagnet. We write the interfacial torque in the form

$$\mathbf{T} = \delta(z) \frac{g\mu_B j_0}{2e} \left[ \tau_d \hat{\mathbf{M}} \times (\hat{\mathbf{M}} \times \hat{\mathbf{y}}) + \tau_f \hat{\mathbf{M}} \times \hat{\mathbf{y}} \right], \quad (14)$$

where  $\delta(z)$  localizes the torque to the interface at  $z = 0$ . The dimensionless coefficients  $\tau_d$  and  $\tau_f$  characterize the “damping-like” and “field-like” contributions respectively. Other terms are possible, as we discuss in Ref. 27, but in the three-dimensional transport calculations we find these other terms to be negligible for the parameters we consider.

The prefactor in Eq.(14) is based on  $j_0$ , which is the “bulk” current density in the non-magnetic layer, that is  $j_0 = \sigma_N E$  where  $E$  is the applied electric field. This choice seems to be that typically made in analyses of experiments even though the total current is all that is directly measurable. The rest of the factors convert from current density to magnetization torque density,  $\hat{\mathbf{M}}$ . This choice makes sense in analyzing experiments in terms of the spin Hall effect because the torque is driven by the current density in the non-magnet. However, for thin films, there can be important corrections due to the outer boundaries and the interface with the ferromagnet. These corrections are shown in Fig. 5 for a variety of thicknesses for the two layers. The average current density is reduced by the diffuse scattering assumed at the outer boundary of the layer, but is increased by the (assumed) higher conductivity of the ferromagnetic layer when that layer is thick enough.

For this model, with no interfacial spin-orbit coupling,

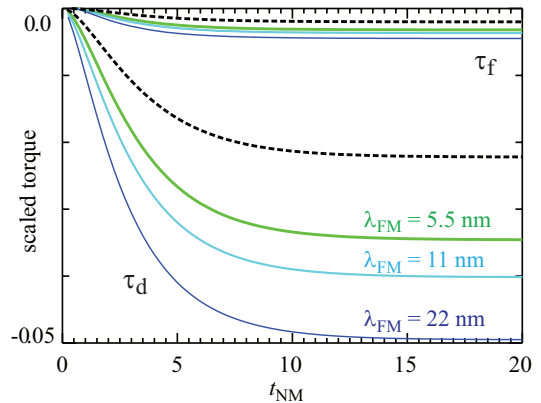


FIG. 6: (color online) Torques as a function of nonmagnetic layer thickness. The solid curves are the full Boltzmann equation calculation and the dashed curves give the analytic approximation based on the drift-diffusion model and the circuit theory (Appendix B). The more negative curves show the field-like torque  $\tau_f$  and those closer to zero show the damping-like torque  $\tau_d$ . For both torques, the Boltzmann results have been calculated for three different mean free paths (labelled on the damping-like torques) in the ferromagnet.

the spin transfer torque is determined solely by the transverse spin current,<sup>68</sup> just outside the magnetic layer. Since neither the majority transmission probability is zero nor the minority reflection probability is one, some of the transverse spin current is reflected. The reflected spin current is seen in the reduction of the transverse spin current close to the interface. Some of the transverse spin current is absorbed right at the interface and some is transmitted into the ferromagnet. In the ferromagnet, spin components transverse to the magnetization rapidly precess as they traverse the layer, as seen in the oscillations in panel (b). Further, different parts of the Fermi surface precess at different rates so they dephase as they traverse the layer as can be seen by the decay of the transverse spin current in the ferromagnet in panel (b).

The dominant spin transfer torque arises from the absorption of the incident transverse spin current either at the interface or in the ferromagnet. However, not all of the current is absorbed, and some is rotated into the  $x$ -component of the spin current on reflection. The non-zero reflection reduces the damping like torque and the rotation gives rise to a small field-like torque. These torques are shown in Fig. 6 as a function of the thickness of the non-magnetic layer.

Figure 6 shows the damping-like and field-like torques calculated with both the Boltzmann equation approach<sup>65</sup> and the drift-diffusion approach. The drift-diffusion approach gives an analytic result, Eq. (B2) in Appendix B. That result is based on the drift-diffusion model described in Sec. III and magnetoelectronic circuit theory<sup>67</sup> for transport across the interface. Both approaches give the same behavior as a function of the thickness of the non-magnetic layer. Because the spin Hall current in the non-magnetic layer is suppressed when the layer is thin,

as seen in Fig. 4, the torque is reduced when the layer thickness is less than a few spin diffusion lengths, which for this set of parameters is  $\ell_N^{\text{sf}} = 2.5$  nm.

For thick layers, the value saturates, but does not saturate to the spin Hall angle  $\theta_{\text{SH}}$  as might be expected. Eq. (B2) shows that for the drift-diffusion model, the saturation value depends on the ratio,  $\ell_N^{\text{sf}}\text{Re}[g^{\uparrow\downarrow}]/\sigma_N$ . When this ratio is small, the saturation value is reduced from  $\theta_{\text{SH}}$  and the Boltzmann calculation and the drift-diffusion calculation saturate to different values. When that ratio is large, the drift-diffusion and Boltzmann equation results agree. However, a large value of this ratio is not physically realistic for systems with strong spin-orbit coupling. The mixing conductance depends mainly on the area of the Fermi surface in the non-magnet (as a reminder our calculations assume the same Fermi surface for all materials), but does so in the same way that the conductivity does (see the expression in Table I, so it is difficult to increase the ratio by changing the mixing conductance. It is possible to decrease the conductivity by increasing the non-spin-flip scattering, but this also decreases the spin-diffusion length. For the default parameters we consider, see Table I, the value of this ratio is about 0.3.

Eq. (B2) also shows that the torque calculated with the drift-diffusion approach is independent of the details of the ferromagnetic layer, depending only on the mixing conductance. The results for the Boltzmann equation, for which we do not have analytic results, do depend on the details of the ferromagnetic layer as seen in Fig. 6 for different values of the mean free path in the ferromagnet. When the mean free path is long so that the conductivity in the ferromagnetic layer is much greater than that in the non-magnetic layer, the current near the interface in the non-magnet is increased (see Fig. 4) giving a greater spin Hall current. Another difference between the approaches is that the only length scale for variation in the drift-diffusion approach is the spin-diffusion length. There are many more length scales in the Boltzmann equation approach (see Table I) and these turn out to play a non-negligible role when  $\ell_N^{\text{sf}}\text{Re}[g^{\uparrow\downarrow}]/\sigma_N$  is not large. The deviation between the results of the Boltzmann equation calculations and those found from the drift-diffusion equation should provide a note of caution for the extraction of physical parameters, like the spin Hall angle, from comparisons between experiment and the drift-diffusion equation.

We conclude that without additional spin-orbit coupling at the interface between the two materials, three-dimensional transport models predict a torque that is predominantly damping-like but has a minor field-like contribution. In the parameter range we have studied, the torque is always well described by the combination of these two forms. The drift-diffusion approach qualitatively captures the physics but can quantitatively fail in physically relevant parameter regimes.

## V. INCLUSION OF INTERFACIAL RASHBA COUPLING

The results in Ref. 27 show that there is an interfacial region with significant spin orbit coupling and exchange splitting. In this section, we model that overlap region by adding a Rashba term to the energy at the interface, see Eq. (10). We find that this additional term primarily leads to a field-like torque and that as long as it is not too strong it does not significantly modify the torques due to the spin Hall effect.

Previously, this region has been treated by two-dimensional calculations in which the electronic structure is modified by the competition between the Rashba interaction and the exchange interaction.<sup>21–24</sup> Typically, the Rashba interaction and the exchange interaction are taken to be very different in magnitude so that the Fermi surfaces remain essentially circular. However, the spin eigendirections on the Fermi surfaces are modified so that the non-equilibrium occupation due to a current flow give rise to a net spin accumulation that is not aligned with the magnetization. This net transverse spin density generates a field-like exchange torque on the magnetization.

In the Boltzmann equation approach that we use, the Rashba interaction modifies the boundary conditions for the distribution functions at the interface. The resulting torque is very similar to what is found in the two-dimensional calculations. Depending on the details of the parameters, the transmission probability is, on average, either greater or lesser for spins aligned with  $\hat{\mathbf{z}} \times \mathbf{j}$  than for those in other directions. The spin density at the interface is determined by the transmission probabilities and the incident fluxes. The bias in the transmission probability favors a net spin polarization aligned with  $\hat{\mathbf{z}} \times \mathbf{j}$ , very similar to the behavior found in the two-dimensional treatments. Then, through Eq. (13), there is a field-like torque.

The effect of introducing the Rashba-term on the current distribution is shown in Fig. 4. Unfortunately, the spin densities at the interface are obscured by the approximations of the Boltzmann equation. In this approach, we assume that electrons on different parts of the Fermi surface are incoherent with each other. However, the matching conditions for the distribution functions across the interface are found through coherent scattering calculations. Once the scattering states are used to construct the matching conditions, the coherence between the incoming and outgoing states is neglected. As a result, for each electron the spin density at the interface is equal to the incident amplitude times either the transmission probability  $|T|^2$  or  $|1 + R|^2$ , which are the same because the wave function is continuous across the interface. However, immediately outside the interface, the incident and reflected states are no longer treated as coherent, on one side of the interface the spin density is proportional to  $|T|^2$  and on the other  $1 + |R|^2$ . Since there are electrons incident from both sides, the spin density at the interface is not equal to the spin density on either

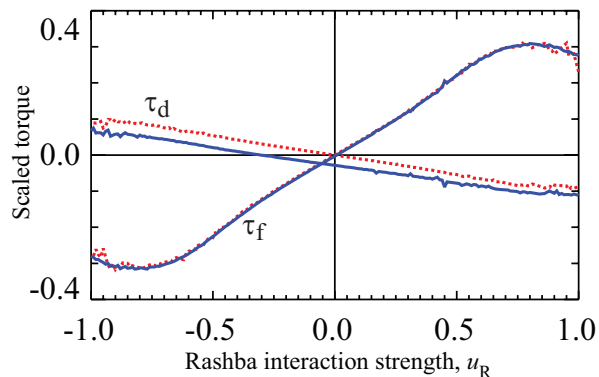


FIG. 7: (color online) Scaled torques as a function of the interfacial Rashba interaction. The solid curves are calculated with a bulk spin Hall effect and the dotted curves without. The non-magnetic layer is 6 nm thick and the ferromagnetic layer is 4 nm. The damping-like and field-like torques are labeled with  $\tau_d$  and  $\tau_f$  respectively. The jitter is due to numerical instabilities.

side.

In Fig. 4, we have used a strength of the Rashba interaction that gives a torque that is comparable to that found from the spin Hall effect. However, this interaction only has a small effect on the spin currents and accumulations. We find that the spin currents for systems with both the spin Hall effect and the interfacial Rashba interaction can be simply and accurately approximated as follows. The currents in the plane, panels a, d, and g in Fig. 4 are essentially the same in all three systems. For system with both the spin Hall effect and the Rashba interaction, the transverse spin currents perpendicular to the plane, panel e in Fig. 4, are a sum of the transverse spin currents found in systems with one effect or the other, panels b and h. The same holds true for the resulting torques, the torques for systems with both effects are approximately the sum of the torques found in the systems with one effect or the other.

The approximate independence of the torques due to the spin Hall effect and the interfacial Rashba interaction is illustrated in Fig. 7 as a function of the strength of the interfacial Rashba interaction. There are contributions to both the field-like and damping-like torques that increase linearly with the Rashba interaction strength up to large values of the torques. Eventually, the transmission probabilities get so low, see Eq. (12), that all electrons are reflected and the torques go to zero. Comparing calculations done with and without the spin Hall effect shows that the interfacial coupling has very little effect on the torque from the spin Hall effect, particularly for small values of the Rashba interaction strength. Without *a priori* knowledge of the parameters of the system, particularly the spin diffusion length, the spin Hall angle, and the interfacial spin-orbit coupling, a wide variety of combinations of damping-like and field-like torques are possible.

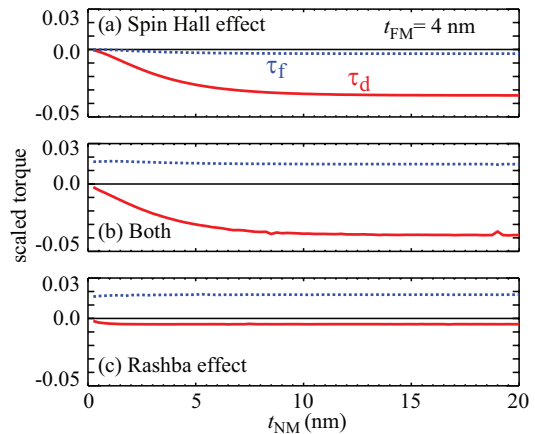


FIG. 8: (color online) Dimensionless torque components as a function of the thickness of the non-magnetic layer. Panel (a) shows the torques in the absence of the Rashba contribution from the interfacial spin-orbit coupling, panel (c) shows the torques in the absence of the spin Hall effect in the non-magnet, and panel (b) shows the torques with both present. In each panel, the solid lines show the damping-like torque and the dotted lines the field-like torque.

Figure 8 shows the torques as a function of the thickness of the non-magnetic layer. The torques due to the spin Hall effect largely depend exponentially on the non-magnetic layer thickness divided by the spin diffusion length. As can be seen from the analytic solution presented in Appendix B, for very small thicknesses there are corrections such that the torque varies as  $t_{\text{NM}}^2$  rather than linearly as it would if the behavior were strictly exponential. The exponential variation has been used<sup>32</sup> to extract the spin diffusion length for particular systems. It is interesting to note that for this simple model, the sign of the product  $\tau_d \tau_f$  is opposite in the two limiting cases, the spin Hall effect only case [Fig. 8(a)] and the Rashba effect only case [Fig. 8(c)].

Figure 9 shows the torque as a function of the ferromagnetic thickness. As expected from the analytic solution in Appendix B that is displayed in Fig 6, the torque due to the spin Hall effect only depends weakly on the thickness of the ferromagnetic layer. The variation is largely due to the variation in the current in the non-magnetic layer due to the presence (and variation) of the ferromagnetic layer. The torque due to the Rashba effect depends more strongly on the ferromagnetic thickness, but not nearly so strongly as is seen in experiment where changing the thickness by a single atomic layer can have a profound effect on the torque.

This discrepancy suggests that the thickness dependence seen in experiment is likely due to physics beyond the scope of the model presented here. One possibility is that the strength of the Rashba interaction could depend sensitively on the thickness of the ferromagnetic layer. The sensitivity could arise from changes in the electronic structure of the interface or even changes in the structure of the interface. Since the lattice mismatch is so large,

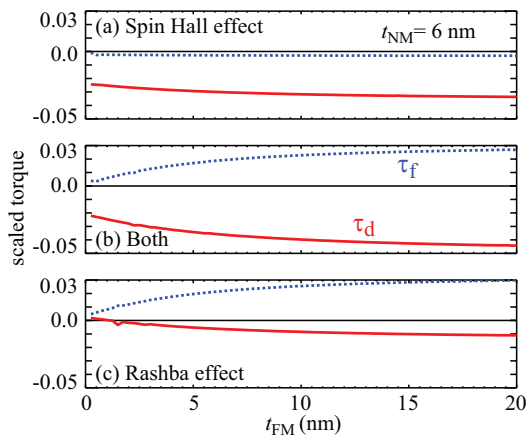


FIG. 9: (color online) Dimensionless torque components as a function of the thickness of the ferromagnetic layer. Panel (a) shows the torques in the absence of the Rashba contribution from the interfacial spin-orbit coupling, panel (c) shows the torques in the absence of the spin Hall effect in the non-magnet, and panel (b) shows the torques with both present. In each panel, the solid lines show the damping-like torque and the dotted lines the field-like torque.

it is conceivable that the structure evolves rapidly as the layer is made thicker.

## VI. SUMMARY

In this article, we have developed semiclassical models for electron and spin transport in bilayer nanowires with a ferromagnetic layer and a non-magnetic layer with strong spin-orbit coupling. We use a Boltzmann equation approach, based on a simplified electronic structure and also a simpler drift-diffusion model. The drift-diffusion framework qualitatively describes the physics of these systems and provides a useful language to discuss their behavior. However, it quantitatively disagrees with the Boltzmann equation to which it is an approximation.

The differences between the results found from the Boltzmann equation and those from the drift-diffusion calculation arise for a couple of reasons. One reason is related to the failure of the drift-diffusion calculation in other cases of in-plane transport. While currents consist of electrons moving in all directions, in the drift-diffusion approximation, that motion in all (three-dimensional) directions is averaged, leaving a single direction for the current. A consequence of this averaging is that the model misses the injection of current and spin current moving parallel to the interface from one layer to the other. In the case of CIP GMR, the lack of injected spin currents flowing from one layer to the other eliminates any CIP GMR. In the present case, the approximation misses the injection of parallel current across the interfaces. The injection (or reduction) of the current flow in the plane of the interface can change the resulting torque by a factor of two or more. Another source of disagreement between

the calculations is that the distribution function has a different form than that assumed when formulating the boundary conditions in the magnetoelectronic circuit theory. The differences between the assumed distribution function and that near the interface in the Boltzmann equation gives quantitative differences between the two.

These models provide a framework that naturally includes both the torques due to the bulk spin Hall effect and the spin transfer torque and the torques due to the interfacial spin-orbit coupling. These two torques are the current induced torques that arise from spin-orbit coupling and which are independent of the gradient of the magnetization. The models we treat are qualitatively similar to previous models for the spin-Hall-induced torque but differ substantially from the models used to describe the Rashba torque. Those latter models are based on a two dimensional treatment of the transport that gives rise to a current induced spin accumulation and a predominantly field-like torque. The Boltzmann equation approach includes the interfacial spin-orbit coupling in the boundary conditions of a three dimensional transport calculation. Nevertheless, this approach gives very similar results to the two-dimensional calculations. The interfacial spin-orbit coupling gives rise to a torque that is predominantly field-like. Depending on the specific parameters appropriate for a particular system, either the field-like torque or the damping-like torque may dominate.

While the experimental situation is still controversial, there is experimental evidence that both a damping-like torque and in some systems a field-like torque play an important role in the dynamics. The model developed here through the Boltzmann equation captures the physics for both. Unfortunately, it is difficult to make the model predictive rather than explanatory. While many of the transport parameters are known for thick films, they are likely to change significantly in thin films. In fact, many vary with varying thicknesses of the films. This model does capture the variation with the thickness of the non-magnetic layer, but does not describe the rapid variation with ferromagnetic film thickness found in some systems. This behavior, coupled with the variation of behavior with the order of growth, suggests to us that structural aspects of the samples vary with thickness or growth order. Examples of process that might contribute to this variation include, interdiffusion, strain relief, or grain size.

## Acknowledgments

Prof. K.-J. Lee acknowledges support under the Cooperative Research Agreement between the University of Maryland and the National Institute of Standards and Technology Center for Nanoscale Science and Technology, Award 70NANB10H193, through the University of Maryland.

## Appendix A: Boltzmann Equation

The Boltzmann equation is a semiclassical approach based on the approximation that in some small but not too small region of space it is possible to define electron wave packets that have both a well defined momentum and a well defined position. It is related to a density matrix approach which neglects all of the coherence between states with different wave vectors. The basic quantity of interest is the distribution function,  $f(\mathbf{k}, \mathbf{r})$ , which is the probability to find an electron with wave vector  $\mathbf{k}$  at position  $\mathbf{r}$ .

The straightforward generalization of the Boltzmann equation for spin polarized systems is to have separate distribution functions for up and down electrons,  $f^\uparrow$  and  $f^\downarrow$ . This is the approach used by Camley and Barnas<sup>60</sup> to model GMR. For systems with spin-orbit coupling, in which spins can point in arbitrary directions, there are two related approaches to generalizing the distribution function. In analogy with the density matrix, the distribution function can be generalized to a  $2 \times 2$  Hermitian matrix in spin space,  $\mathbf{f}$ . Alternatively, the same information can be captured by four real distribution functions  $f_\alpha$ ,  $\alpha = 0, x, y, z$  related to  $\mathbf{f}$  by

$$f_\alpha = \text{Tr}[\sigma_\alpha \mathbf{f}], \quad (\text{A1})$$

where

$$\sigma_0 = \begin{pmatrix} 1 & 0 \\ 0 & 1 \end{pmatrix} = \text{I} \quad (\text{A2})$$

$$\sigma_x = \begin{pmatrix} 0 & 1 \\ 1 & 0 \end{pmatrix} \quad (\text{A3})$$

$$\sigma_y = \begin{pmatrix} 0 & -i \\ i & 0 \end{pmatrix} \quad (\text{A4})$$

$$\sigma_z = \begin{pmatrix} 1 & 0 \\ 0 & -1 \end{pmatrix} \quad (\text{A5})$$

$$\boldsymbol{\sigma} = (\sigma_x, \sigma_y, \sigma_z) \quad (\text{A6})$$

The generalized Boltzmann equation is

$$\begin{aligned} & \frac{\partial f_\alpha}{\partial t} + \frac{d\mathbf{r}}{dt} \frac{\partial f_\alpha}{\partial \mathbf{r}} + \frac{d\mathbf{k}}{dt} \frac{\partial f_\alpha}{\partial \mathbf{k}} + \gamma H_\beta^{\text{ex}} f_\gamma \epsilon_{\alpha\beta\gamma} \\ & = \frac{df_\alpha}{dt}_{\text{coll}} [f_\beta(t, \mathbf{r}, \mathbf{k}, n)], \end{aligned} \quad (\text{A7})$$

where the collision term on the right hand side depends on all four distribution functions. The last term on the left hand side describes spin precession in ferromagnetic layers, where the electron spins precess in the exchange field  $\mathbf{H}^{\text{ex}}$ . The time derivatives of  $\mathbf{r}$  and  $\mathbf{k}$  are given by

$$\frac{d\mathbf{r}}{dt} = \mathbf{v}_{\mathbf{k},n} \quad (\text{A8})$$

$$\hbar \frac{d\mathbf{k}}{dt} = -e\mathbf{E}, \quad (\text{A9})$$

where  $\mathbf{v}_{\mathbf{k},n}$  is the velocity of the electron and  $\mathbf{E}$  is the electric field. For the linearized Boltzmann equation, we make the replacement

$$f_\alpha(\mathbf{k}) \rightarrow f_{\text{eq}}(\epsilon(\mathbf{k}))\delta_{\alpha,0} + g_\alpha(\mathbf{K})f'_{\text{eq}}(\epsilon(\mathbf{k})), \quad (\text{A10})$$

Upper case  $\mathbf{K}$  refers to wave vectors restricted to the Fermi surface.  $f'_{\text{eq}}$  is the energy derivative of the Fermi function, emulating a Taylor series expansion of the distribution function around equilibrium.

After some standard algebra, the linearized Boltzmann equation can be cast into the form

$$\left[ \mathbf{v}_{\mathbf{K}} \cdot \frac{\partial g_\alpha(\mathbf{K}_i)}{\partial \mathbf{r}} - e\mathbf{E} \cdot \mathbf{v}_{\mathbf{K}} \delta_{\alpha,0} + \gamma H_\beta^{\text{eff}} g_\gamma(\mathbf{K}) \epsilon_{\alpha\beta\gamma} \right] = -R_{\alpha,\alpha'}(\mathbf{K}_i) g_{\alpha'}(\mathbf{K}_i) + \int_{\text{FS}} d\hat{\mathbf{K}}_f P_{\alpha,\alpha'}(\mathbf{K}_i, \mathbf{K}_f) g_{\alpha'}(\mathbf{K}_f) \quad (\text{A11})$$

The first term on the right hand side is the scattering out term and the second term is the scattering in term. The former describes collision processes that reduce the occupancy of a state and the latter those that increase it.

In the ferromagnet, where we neglect spin-orbit coupling, the scattering is diagonal in a coordinate system aligned with the magnetization. For the magnetization pointing in a general direction  $(\sin \theta \cos \phi, \sin \theta \sin \phi, \cos \theta)$ , the spin-dependent scattering matrix for the scattering out terms is

$$R_{\alpha,\alpha'} = U_{\alpha,\beta}^T R_\beta^{\text{diag}} \delta_{\beta,\beta'} U_{\beta',\alpha'}. \quad (\text{A12})$$

The diagonal scattering matrix is

$$R^{\text{diag}} = (R^\uparrow, \overline{R}, \overline{R}, R^\downarrow), \quad (\text{A13})$$

in terms of the majority and minority scattering rate  $R^\uparrow = 1/\tau^\uparrow$  and  $R^\downarrow = 1/\tau^\downarrow$ , and the transverse scattering rate

is taken to be the geometric mean of the spin-dependent scattering  $\bar{R} = 1/\sqrt{\tau^\uparrow\tau^\downarrow}$ . The transformation matrix is

$$U = \begin{pmatrix} 1/\sqrt{2} & 0 & 0 & 1/\sqrt{2} \\ 0 & 1 & 0 & 0 \\ 0 & 0 & 1 & 0 \\ 1/\sqrt{2} & 0 & 0 & -1/\sqrt{2} \end{pmatrix} \begin{pmatrix} 1 & 0 & 0 & 0 \\ 0 & \cos\theta & 0 & -\sin\theta \\ 0 & 0 & 1 & 0 \\ 0 & \sin\theta & 0 & \cos\theta \end{pmatrix} \begin{pmatrix} 1 & 0 & 0 & 0 \\ 0 & \cos\phi & -\sin\phi & 0 \\ 0 & \sin\phi & \cos\phi & 0 \\ 0 & 0 & 0 & 1 \end{pmatrix} \quad (\text{A14})$$

The first matrix transforms between the majority/minority description on one hand and the Cartesian description that is used in the rest of the calculations. The second two matrices rotate the coordinate system.

The scattering in terms are similar. For these terms, where spin-orbit coupling does not play a role,  $P_{\alpha,\alpha'}$  is independent of wave vector and equal to  $R_{\alpha,\alpha'}$ . There is an additional contribution from spin flip scattering of the form  $R^{\text{sf}}\delta_{\alpha,\alpha'}(1-\delta_{\alpha,0})$  in terms of the spin flip scattering rate  $R^{\text{sf}} = 1/\tau_{\text{sf}}$ . The last factor restricts the scattering to the spin distribution functions and not the charge function.

In the non-magnet, the spin independent scattering is included through a term of the form  $R^{\text{N}}\delta_{\alpha,\alpha'}$  in terms of the scattering rate  $R^{\text{N}} = 1/\tau$ , and spin-flip scattering through a term of the form  $R^{\text{Nsf}}\delta_{\alpha,\alpha'}(1-\delta_{\alpha,0})$  in terms of the spin flip scattering rate  $R^{\text{Nsf}} = 1/\tau_{\text{sf}}$ .

Spin-orbit scattering is more complicated than the scattering processes described above because the scattering rates depends on the initial and final momenta. Engel et al.<sup>36</sup> give the contribution to the collision integral as

$$\begin{aligned} \frac{df}{dt}_{\text{sH}} &= \frac{n_i \hbar k_{\text{F}}}{m^*} \sum_{\mathbf{k}_f} \frac{d\sigma}{d\Omega} [f(\mathbf{k}_i) - f(\mathbf{k}_f)] \\ &= n_i \sum_{\mathbf{k}_f} \frac{\hbar k}{m^*} \left[ I(\varphi) [f(\mathbf{k}_i) - f(\mathbf{k}_f)] \right. \\ &\quad \left. - I(\varphi) S(\varphi) \boldsymbol{\sigma} \cdot \frac{\mathbf{k}_i \times \mathbf{k}_f}{|\mathbf{k}_i \times \mathbf{k}_f|} [f_0(\mathbf{k}_i) + f_0(\mathbf{k}_f)] \right], \end{aligned} \quad (\text{A15})$$

where  $\varphi$  is the angle between  $\mathbf{k}_i$  and  $\mathbf{k}_f$ . This form is based on assuming that the spin-orbit scattering is weak and only keeping quantities lowest order in the spin-flip scattering. We follow this approximation but also include the scattering that gives the inverse spin Hall effect. The complete story is much more complicated because there is also scattering between different spin channels. We assume that  $I(\varphi)$  is a constant and that  $S(\varphi) = S|\mathbf{k}_i \times \mathbf{k}_f|$ , where  $S$  is now a constant. Then, in our notation, we have

$$\begin{aligned} \frac{df_\alpha}{dt}_{\text{sH}} &= n_i \sum_{\mathbf{k}_f} \frac{\hbar k}{m^*} [I[f_\alpha(\mathbf{k}_i) - f_\alpha(\mathbf{k}_f)] \\ &\quad - ISn_\alpha [f_0(\mathbf{k}_i) + f_0(\mathbf{k}_f)] \\ &\quad + IS\delta_{\alpha,0}n_{\alpha'} [f_{\alpha'}(\mathbf{k}_i) + f_{\alpha'}(\mathbf{k}_f)]] \\ &= \sum_{\mathbf{k}_f} [-ISn_\alpha f_0(\mathbf{k}_f) + IS\delta_{\alpha,0}n_{\alpha'} f_{\alpha'}(\mathbf{k}_f)] \end{aligned} \quad (\text{A16})$$

where  $\mathbf{n} = \mathbf{k}_i \times \mathbf{k}_f$  or  $n_\alpha = \epsilon_{\alpha,\beta,\gamma}k_i\beta k_f\gamma$ . The terms con-

taining  $\delta_{\alpha,0}$  are the additional terms that give the inverse spin Hall effect. In the second step, we have dropped the isotropic part because it is simply another contribution to the isotropic scattering. We also find that for the remaining parts, the scattering out contribution is zero because  $\sum_f n_\alpha = 0$ . Finally, we absorbed the velocity and the impurity density factor into the scattering rate. Translating to the notation we have been using gives

$$P_{\alpha,\alpha'} = PS[k_{i\beta}k_{f\gamma}\epsilon_{\alpha,\beta,\gamma}\delta_{\alpha',0} - k_{i\beta}k_{f\gamma}\epsilon_{\alpha',\beta,\gamma}\delta_{\alpha,0}] \quad (\text{A17})$$

Given the scattering matrices, we find the general solutions of the Boltzmann equation in each layer using the techniques described in Ref. 63. These are matched together at the interface through boundary conditions based on Eq. (10) and Eq. (12) and subjected to diffuse or specular boundary conditions at the out interfaces.

The default values of the parameters we use are given in Table I. These have been chosen to approximately have values appropriate for Co/Pt bilayers with vacuum on either side. These parameters are either input parameters, calculated numerically based on the input parameters or determined analytically from them. In the last case, the evaluated expression is given in the table.

## Appendix B: Analytical expression based on circuit theory

In this Section, we present an analytical expression of spin torque caused by the spin Hall effect (only) in NM|FM bilayer structures where NM has strong spin-orbit coupling and is thus subject to the spin Hall effect. The derivation is based on the drift-diffusion model<sup>64</sup> with the boundary condition of the magnetoelectronic circuit theory.<sup>67</sup> This result does not account for Rashba-like interactions at the interface but provides a closed-form result in their absence.

The bulk transport is determined by Eqs.(2-8) and the current across the interface is calculated using magnetoelectronic circuit theory.<sup>67,73</sup> The charge and spin currents satisfy the boundary conditions at the NM|FM boundary ( $z = 0$ ) given by

$$\begin{aligned} j_z &= (G^\uparrow + G^\downarrow)\Delta\mu - (G^\uparrow - G^\downarrow)\Delta\boldsymbol{\mu}_s \cdot \hat{\mathbf{M}} \\ \hat{\mathbf{z}} \cdot \mathbf{Q} &= \text{Re}[G^{\uparrow\downarrow}](2\Delta\boldsymbol{\mu}_s \times \hat{\mathbf{M}} \times \hat{\mathbf{M}}) - \text{Im}[G^{\uparrow\downarrow}](2\Delta\boldsymbol{\mu}_s \times \hat{\mathbf{M}}) \\ &\quad - (G^\uparrow + G^\downarrow)\Delta\boldsymbol{\mu}_s + (G^\uparrow - G^\downarrow)\Delta\boldsymbol{\mu}\hat{\mathbf{M}}, \end{aligned} \quad (\text{B1})$$

TABLE I: Default parameter values. Parameters for the ferromagnet (F), are chosen to be roughly those for Co as in Ref. 72 and those for the non-magnet (N), to be roughly those for Pt as in Ref. 32.  $\lambda = v_F \tau$  is a mean free path and  $\ell^{sf}$  is a spin diffusion length. The rest of the parameters are defined in the text.

$\lambda_N$	input	2.43 nm
$\lambda_N^{sf}$	input	14.7 nm
$\lambda_{SH}$	input	11.8 nm
$\lambda_N^\uparrow$	input	16.25 nm
$\lambda_N^\downarrow$	input	6.01 nm
$\lambda_F^{sf}$	input	3280 nm
$\lambda_{ex}$	input	0.258 nm
$k_F$	input	16 nm <sup>-1</sup>
$u_0$	input	0.42645
$u_{ex}$	input	0.20055
$u_R$	input	0.04
$\theta_{SH}$	computed	-0.059
$\ell_N^{sf}$	computed	2.57 nm
$\ell_F^{sf}$	computed	69.3 nm
$\sigma_N$	$\frac{e^2}{h} \frac{2\lambda_N}{3\pi^2} \pi k_F^2$	0.005 nm <sup>-1</sup> Ω <sup>-1</sup>
$\rho_N$	$1/\sigma_N$	20 μΩcm
$\sigma_F$	$\frac{e^2}{h} \frac{\lambda_F^\uparrow + \lambda_F^\downarrow}{3\pi^2} \pi k_F^2$	0.02 nm <sup>-1</sup> Ω <sup>-1</sup>
$\rho_F$	$1/\sigma_F$	5 μΩcm
$G^\uparrow$	evaluated	$6.66 \times 10^{14}$ Ω <sup>-1</sup> m <sup>-2</sup>
$G^\downarrow$	evaluated	$3.96 \times 10^{14}$ Ω <sup>-1</sup> m <sup>-2</sup>
$\text{Re}[G^{\uparrow\downarrow}]$	evaluated	$5.94 \times 10^{14}$ Ω <sup>-1</sup> m <sup>-2</sup>
$\text{Im}[G^{\uparrow\downarrow}]$	evaluated	$0.86 \times 10^{14}$ Ω <sup>-1</sup> m <sup>-2</sup>

where  $G^\uparrow$  and  $G^\downarrow$  are interface conductances for majority and minority spins, aligned antiparallel and parallel to  $\mathbf{M}$  respectively,  $G^{\uparrow\downarrow}$  is the mixing conductance,  $\Delta\mu = \mu(z = +0) - \mu(z = -0)$  is the chemical potential drop over the interface, and  $\Delta\mu_s$  is the spin chemical potential drop across the interface.

By solving the bulk equations, Eqs.(2-8), the boundary conditions at the interface between the materials, Eq. (B1), with the additional boundary conditions,  $j_z = 0$  at  $z = 0$ , and  $\mathbf{j}_s = 0$  at  $z = +t_F$  and  $z = -t_N$ , where  $t_F$  and  $t_N$  are the thicknesses of FM and NM, respectively, one obtains coefficients for two vector components of spin torque as in Eq. (14)

$$\tau_d = \theta_{SH} 2(\kappa_N - 1)^2 l_{sf}^N \frac{2\text{Im}[G^{\uparrow\downarrow}]^2 (1 + \kappa_N^2) l_{sf}^N + \text{Re}[G^{\uparrow\downarrow}] [2(1 + \kappa_N^2) l_{sf}^N \text{Re}[G^{\uparrow\downarrow}] + (1 - \kappa_N^2) \sigma_N]}{[2\text{Im}[G^{\uparrow\downarrow}] (1 + \kappa_N^2) l_{sf}^N]^2 + [2(1 + \kappa_N^2) l_{sf}^N \text{Re}[G^{\uparrow\downarrow}] + (1 - \kappa_N^2) \sigma_N]^2} \quad (\text{B2})$$

$$\tau_f = \theta_{SH} 2(\kappa_N - 1)^2 l_{sf}^N \frac{\text{Im}[G^{\uparrow\downarrow}] (1 - \kappa_N^2) \sigma_N}{[2\text{Im}[G^{\uparrow\downarrow}] (1 + \kappa_N^2) l_{sf}^N]^2 + [2(1 + \kappa_N^2) l_{sf}^N \text{Re}[G^{\uparrow\downarrow}] + (1 - \kappa_N^2) \sigma_N]^2}, \quad (\text{B3})$$

where  $\theta_{SH} = \sigma_{SH}/\sigma_N$  is the spin Hall angle,  $\sigma_N$  is the conductivity of NM,  $\kappa_N = \exp(-t_N/l_{sf}^N)$ , and  $l_{sf}^N$  is the spin diffusion length of NM. We note that both  $\tau_d$  and  $\tau_f$  do not depend on the magnetization direction for the case with the spin Hall effect only. Thus for the case with the spin Hall effect only, the angular dependence of the torque on the magnetization direction is completely determined by the cross products in Eq. (14). These damping and field like torques are plotted in Fig. (6) (dashed lines). These results are independent of the thickness of the ferromagnetic layer because the boundary conditions force the transverse spin current to be zero in the ferromagnet. All of the dependence of the non-magnetic layer thickness is captured in the factors of  $\kappa_N$ .

The mixing conductance in Eq. (B2) and Eq. (B3) is evaluated by the integral<sup>67</sup>

$$G^{s,-s} = \frac{e^2}{h} \int_{\text{FS}} \frac{d^2 k}{(2\pi)^2} (1 - r_s r_{-s}^*). \quad (\text{B4})$$

Here, “up” and “down” spins are defined with respect to the magnetization, so that  $s = 1$  corresponds to a minority electron with its spin parallel and moment antiparallel to the magnetization. FS refers to integrating over the Fermi surface. The mixing conductance becomes

$$G^{\uparrow\downarrow} = \frac{e^2}{h} \int_{\text{FS}} \frac{d^2 k}{(2\pi)^2} (1 - r_\downarrow r_\uparrow^*). \quad (\text{B5})$$

On the right hand side,  $\uparrow$  and  $\downarrow$  refer to majority and minority electrons respectively. For the model treated here, with a delta function sheet potential, Eq. (12) gives the reflection amplitudes, so the mixing conductance becomes

$$\begin{aligned}
 G^{\uparrow\downarrow} &= \frac{e^2 k_F^2}{2\pi h} \int_0^1 dx x \left( 1 - \frac{u^\downarrow}{ix - u^\downarrow} \frac{u^\uparrow}{-ix - u^\uparrow} \right) \\
 &= \frac{e^2 k_F^2}{2\pi h} \left\{ \frac{1}{2} + \frac{u^\uparrow u^\downarrow}{2(u^\uparrow + u^\downarrow)} \left[ u^\downarrow \ln \left( \frac{u^{\downarrow 2}}{1 + u^{\downarrow 2}} \right) + u^\uparrow \ln \left( \frac{u^{\uparrow 2}}{1 + u^{\uparrow 2}} \right) \right] \right. \\
 &\quad \left. + i \frac{u^\uparrow u^\downarrow}{2(u^\uparrow + u^\downarrow)} \left[ u^\downarrow (\pi - 2 \tan^{-1}(u^\downarrow)) - u^\uparrow (\pi - 2 \tan^{-1}(u^\uparrow)) \right] \right\}. \tag{B6}
 \end{aligned}$$

Here  $u^\downarrow = u_0 - u_{\text{ex}}$  and  $u^\uparrow = u_0 + u_{\text{ex}}$ . If  $u^\downarrow > u^\uparrow$  as is the case here, both the real and the imaginary parts of the mixing conductance are positive.

- 
- <sup>1</sup> L. Liu, C.-F. Pai, Y. Li, H. W. Tseng, D. C. Ralph and R. A. Buhrman, *Science* **4**, 555 (2012).
- <sup>2</sup> I. M. Miron, T. Moore, H. Szambolics, L. D. Buda-Prejbeanu, S. Auffret, B. Rodmacq, S. Pizzini, J. Vogel, M. Bonfim, A. Schuhl and G. Gaudin, *Nature Materials* **10**, 419 (2011).
- <sup>3</sup> E. van der Bijl and R. A. Duine, *Phys. Rev. B* **86**, 094406 (2012).
- <sup>4</sup> L. Berger, *J. Appl. Phys.* **3**, 2156 (1978); *ibid.* **3**, 2137 (1979).
- <sup>5</sup> L. Berger, *J. Appl. Phys.* **55**, 1954 (1984).
- <sup>6</sup> S. Zhang and Z. Li, *Phys. Rev. Lett.* **93**, 127204 (2004).
- <sup>7</sup> G. Tatara, H. Kohno, *Phys. Rev. Lett.* **92**, 086601 (2004).
- <sup>8</sup> A. Thiaville, Y. Nakatani, J. Miltat, and Y. Suzuki, *Europhys. Lett.* **69**, 990 (2005).
- <sup>9</sup> Y. Tserkovnyak, A. Brataas, G. E. W. Bauer, *J. Magn. Magn. Mater.*, **320**, 1282 (2008).
- <sup>10</sup> G. Tatara, H. Kohno, and J. Shibata, *Phys. Rep.* **468**, 213 (2008).
- <sup>11</sup> J. Shibata, G. Tatara, H. Kohno, *J. Phys. D* **44**, 384004 (2011).
- <sup>12</sup> K. Ando, S. Takahashi, K. Harii, K. Sasage, J. Ieda, S. Maekawa, and E. Saitoh, *Phys. Rev. Lett.* **101**, 036601 (2008).
- <sup>13</sup> J. E. Hirsch, *Phys. Rev. Lett.* **83**, 1834 (1999).
- <sup>14</sup> S. F. Zhang, *Phys. Rev. Lett.* **85**, 393 (2000).
- <sup>15</sup> J. Sinova, D. Culcer, Q. Niu, N. A. Sinitsyn, T. Jungwirth, and A. H. MacDonald, *Phys. Rev. Lett.* **92**, 126603 (2004).
- <sup>16</sup> S. Murakami, N. Nagaosa, and S. C. Zhang, *Science* **301**, 1348 (2003).
- <sup>17</sup> J. Slonczewski, *J. Magn. Magn. Mat.* **62**, 123, (1996).
- <sup>18</sup> L. Berger, *Phys. Rev. B* **54**, 9353 (1996).
- <sup>19</sup> M. D. Stiles and J. Miltat, *Top. Appl. Phys.* **101**, 225 (2006).
- <sup>20</sup> D. C. Ralph and M. D. Stiles, *J. Magn. Magn. Mater.* **320**, 1190 (2007).
- <sup>21</sup> K. Obata, and G. Tatara, *Phys Rev. B* **77**, 214429 (2008).
- <sup>22</sup> A. Manchon and S. Zhang, *Phys. Rev. B* **78**, 212405 (2008).
- <sup>23</sup> A. Manchon and S. Zhang, *Phys. Rev. B.* **79**, 094422 (2009).
- <sup>24</sup> A. Matos-Abiague and R. L. Rodriguez-Suarez, *Phys. Rev. B* **80**, 094424 (2009).
- <sup>25</sup> Yu. A. Bychkov and E. I. Rashba, *JETP. Lett.* **39**, 78(1984).
- <sup>26</sup> Strictly speaking, a torque acts on an angular momentum and has units of angular momentum per time. Here we use “torques” to describe contributions to the Landau-Lifshitz-Gilbert equation,  $\dot{\mathbf{M}} = -\gamma\mu_0\mathbf{M} \times \mathbf{H} + \alpha\dot{\mathbf{M}} \times \mathbf{M} + \mathbf{T}$ . As such, they have units of magnetization per time [ $\text{Am}^{-1}\text{s}^{-1}$  instead of energy [J].
- <sup>27</sup> K.-J. Lee, H.-W. Lee, A. Manchon, P. M. Haney, and M. D. Stiles, (to be published)
- <sup>28</sup> R. Lavrijsen, P. P. J. Haazen, E. Mur, J. H. Franken, J. T. Kohlhepp, H. J. M. Swagten, and B. Koopmans, *Appl. Phys. Lett.* **100**, 262408 (2012)
- <sup>29</sup> S. S. P. Parkin (unpublished).
- <sup>30</sup> L. Liu, T. Moriyama, D. C. Ralph, and R. A. Buhrman, *Phys. Rev. Lett.* **106**, 036601 (2011).
- <sup>31</sup> L. Liu, O. J. Lee, T. J. Gudmundsen, D. C. Ralph, and R. A. Buhrman, *Phys. Rev. Lett.* **109**, 096602 (2012).
- <sup>32</sup> L. Liu, R. A. Buhrman, D. C. Ralph, arXiv:1111.3702.
- <sup>33</sup> I. M. Miron, G. Gaudin, S. Auffret, B. Rodmacq, A. Schuhl, S. Pizzini, J. Vogel and P. Gambardella, *Nature Materials* **9**, 230 (2010).
- <sup>34</sup> I. M. Miron, K. Garello, G. Gaudin, P.-J. Zermatten, M. V. Costache, S. Auffret, S. Bandiera, B. Rodmacq, A. Schuhl, and P. Gambardella, *Nature (London)* **476**, 189 (2011).
- <sup>35</sup> Y. K. Kato, R. C. Myers, A. C. Gossard, and D. D. Awschalom, *Science* **306**, 1910 (2004).
- <sup>36</sup> H.-A. Engel, B. I. Halperin, and E. I. Rashba, *Phys. Rev. Lett.* **95**, 166605 (2005).
- <sup>37</sup> C.-F. Pai, L. Liu, Y. Li, H. W. Tseng, D. C. Ralph, R. A. Buhrman, *Appl. Phys. Lett.* **101**, 122404 (2012).
- <sup>38</sup> The corresponding equation (1) in Ref. 33 is larger than Eq. (1) in our paper by factor 2. Equation (1) in Ref. 33 is quoted from the theoretical work,<sup>22</sup> which however contains a factor 2 error. When this error is corrected, it results in Eq. (1) in our paper.
- <sup>39</sup> Reference 33 reported  $\alpha_R \approx 0.1$  eVnm, which is factor 2 smaller than the value quoted in our paper. However Eq. (1) in Ref. 33 is wrong<sup>38</sup> by factor 2 and when this error is corrected, the proportionality constant  $(1.0 \pm 0.1) \times 10^{-12}$  T/(Am<sup>-2</sup>) implies  $\alpha_R \approx 0.2$  eVnm as stated in our paper.

- <sup>40</sup> C. R. Ast, J. Henk, A. Ernst, L. Moreschini, M. C. Falub, D. Pacilé, P. Bruno, K. Kern, and M. Grioni, *Phys. Rev. Lett.* **98**, 186807 (2007).
- <sup>41</sup> J.-H. Park, C. H. Kim, H.-W. Lee, and J. H. Han, *Phys. Rev. B* **87**, 041301 (2013).
- <sup>42</sup> M. Hayashi, L. Thomas, C. Rettner, R. Moriya, Y. B. Bazaliy, and S. S. P. Parkin, *Phys. Rev. Lett.* **98**, 037204 (2007).
- <sup>43</sup> G. S. D. Beach, C. Nistor, C. Knutson, M. Tsoi, and J. L. Erskine, *Nature Mater.* **4**, 741 (2005).
- <sup>44</sup> N. L. Schryer and L. R. Walker, *J. Appl. Phys.* **45**, 5406 (1974).
- <sup>45</sup> A. Yamaguchi, T. Ono, S. Nasu, K. Miyake, K. Mibu, T. Shinjo, *Phys. Rev. Lett.* **92**, 077205 (2004).
- <sup>46</sup> M. Yamanouchi, D. Chiba, F. Matsukura, and H. Ohno, *Nature (London)* **428**, 539 (2004).
- <sup>47</sup> K.-W. Kim, S. M. Seo, J. Ryu, K.-J. Lee, and H.-W. Lee, *Phys. Rev. B* **85**, 180404 (2012).
- <sup>48</sup> S.-M. Seo, K.-W. Kim, J. Ryu, H.-W. Lee, and K.-J. Lee, *Appl. Phys. Lett.* **101**, 022405 (2012).
- <sup>49</sup> X. Wang and A. Manchon, *Phys. Rev. Lett.* **108**, 117201 (2012).
- <sup>50</sup> D. A. Pesin and A. H. MacDonald, *Phys. Rev. B* **86**, 014416 (2012).
- <sup>51</sup> U. H. Pi, K. W. Kim, J. Y. Bae, S. C. Lee, Y. J. Cho, K. S. Kim, and S. Seo, *Appl. Phys. Lett.* **97**, 162507 (2010).
- <sup>52</sup> T. Suzuki, S. Fukami, N. Ishiwata, M. Yamanouchi, S. Ikeda, N. Kasai, and H. Ohno, *Appl. Phys. Lett.* **98**, 142505 (2011).
- <sup>53</sup> J. Kim, J. Sinha, M. Hayashi, M. Yamanouchi, S. Fukami, T. Suzuki, S. Mitani, H. Ohno, arXiv:1207.2521.
- <sup>54</sup> P. P. J. Haazen, E. Muré, J. H. Franken, R. Lavrijsen, H. J. M. Swagten, and B. Koopman, arXiv:1209.2320.
- <sup>55</sup> J.-C. Lee, K.-J. Kim, J. Ryu, K.-W. Moon, S.-J. Yun, G.-H. Gim, K.-S. Lee, K.-H. Shin, H.-W. Lee, and S.-B. Choe, *Phys. Rev. Lett.* **107**, 067201 (2011).
- <sup>56</sup> T. Ono (unpublished).
- <sup>57</sup> G. Beach (unpublished).
- <sup>58</sup> A. Thiaville, S. Rohart, É. Jué, V. Cros, and A. Fert, arXiv:1211.5970.
- <sup>59</sup> I. E. Dzialoshinskii, *Sov. Phys. JETP* **5**, 1259 (1957); 14 T. Moriya, *Phys. Rev.* **120**, 91 (1960).
- <sup>60</sup> R. E. Camley and J. Barnaś, *Phys. Rev. Lett.* **63**, 664 (1989).
- <sup>61</sup> T. Valet and A. Fert, *Phys. Rev. B* **48** 7099 (1993).
- <sup>62</sup> J. E. Hirsch, *Phys. Rev. Lett.* **83**, 1834 (1999); S. Zhang, *Phys. Rev. Lett.* **85**, 393 (2000).
- <sup>63</sup> J. Xiao, A. Zangwill, and M. D. Stiles, *European Phys. J. B* **59**, 415 (2007).
- <sup>64</sup> R. V. Shchelushkin and A. Brataas, *Phys. Rev. B* **72**, 073110 (2005); R. V. Shchelushkin and A. Brataas *Phys. Rev. B* **73**, 169907(E) (2006).
- <sup>65</sup> The Boltzmann equation calculations reported in Fig. 6 expand the distribution function in a grid of 8 polar angles and 16 azimuthal angles, or 128 total points. Increasing the number of grid points to 16 polar angles and 20 azimuthal angles (320 total points) gives a root mean square difference between the calculations of less than  $1 \times 10^{-4}$ .
- <sup>66</sup> M. D. Stiles and D. R. Penn, *Phys. Rev. B* **61**, 3200 (2000).
- <sup>67</sup> A. Brataas, Y.V. Nazarov, and G.E.W. Bauer *Phys. Rev. Lett.* **84**, 2481 (2000); A. Brataas, G. E. W. Bauer, P. J. Kelly, *Phys. Rep.* **427**, 157 (2006).
- <sup>68</sup> M. D. Stiles and A. Zangwill, *Phys. Rev. B* **66**, 014407 (2002).
- <sup>69</sup> E. M. Pugh and N. Rostoker, *Rev. Mod. Phys.* **25**, 151 (1953); C. M. Hurd, 1972, *The Hall Effect in Metals and Alloys* Plenum, New York; N. A. Sinitsyn, *J. Phys. Cond. Mat.* **20**, 023201 (2008); N. Nagaosa, J. Sinova, S. Onoda, A. H. MacDonald, N. P. Ong, *Rev. Mod. Phys.* **82**, 1539 (2010).
- <sup>70</sup> T. Tanaka, H. Kontani, M. Naito, T. Naito, D. S. Hirashima, K. Yamada, and J. Inoue, *Phys. Rev. B* **77**, 165117 (2008).
- <sup>71</sup> M. Gradhand, D. V. Fedorov, P. Zahn, and I. Mertig, *Phys. Rev. Lett.* **104**, 186403 (2010).
- <sup>72</sup> J. Bass and W. P. Pratt, *J. Magn. Magn. Mater.* **200**, 274 (1999).
- <sup>73</sup> A. Brataas, Y. V. Nazarov, and G. E. W. Bauer, *Eur. Phys. J. B* **22**, 99 (2001).